On the color structure of Yang-Mills theory with static sources in a periodic box

L. Giusti[a], A. L. Guerrieri[b], S. Petrarca[c], A. Rubeo[d], M. Testa[c]

[a] *Dipartimento di Fisica and INFN, Università di Milano-Bicocca, Piazza della Scienza 3, I-20126 Milano, Italy*

[b] *Dipartimento di Fisica and INFN, Università di Roma Tor Vergata, Via della Ricerca Scientifica 1, I-00133 Roma, Italy*

[c] *Dipartimento di Fisica and INFN, Università di Roma La Sapienza, P.le Aldo Moro 5, I-00185 Roma, Italy*

[d] *School of Mathematics, Trinity College, Dublin 2, Ireland*

We present an exploratory numerical study on the lattice of the color structure of the wave functionals of the SU(3) Yang-Mills theory in the presence of a $q\bar{q}$ static pair. In a spatial box with periodic boundary conditions we discuss the fact that all states contributing to the Feynman propagation kernel are global color singlets. We confirm this numerically by computing the correlations of gauge-fixed Polyakov lines with color-twisted boundary conditions in the time direction. The values of the lowest energies in the color singlet and octet external source sectors agree within statistical errors, confirming that both channels contribute to the lowest (global singlet) state of the Feynman kernel. We then study the case of homogeneous boundary conditions in the time direction for which the gauge-fixing is not needed. In this case the lowest energies extracted in the singlet external source sector agree with those determined with periodic boundary conditions, while in the octet sector the correlator is compatible with being null within our statistical errors. Therefore consistently only the singlet external source contribution has a non-vanishing overlap with the null-field wave functional.

I. INTRODUCTION

The knowledge of the energy levels containing infinitely heavy external sources, immersed in the quantum state of a pure Yang-Mills theory, is useful to understand the full QCD case [1–9]. In Ref. [10] the structure of the states in presence of external sources is analyzed on general grounds, within the temporal gauge, based on the formulation of Refs [11–14]. In particular it is shown how to define projectors on states which are irreducible representations of the global color symmetry, and on states where the external sources are in a given color singlet or octet representation. The last ones are not, in general, eigenstates of the Hamiltonian. This fact led to some confusion in the literature, since a state with a definite global color behavior has non-trivial projections on both singlet and octet external source sectors.

It is one of the aims of this paper to clarify this issue: we show that, when the theory is quantized in a finite space volume with periodic boundary conditions, Gauss's law enforces all states to be global color singlets. We also study in detail the properties of the ground state in presence of a static $q\bar{q}$ pair, and find that its wave functional projects both on the quark-singlet and on the quark-octet external source sectors. When homogeneous boundary conditions in the time direction are chosen, the lowest energies extracted in the singlet external source sector agree with those determined with periodic boundary conditions, while in the octet sector the correlator is consistently compatible with being null within statistical errors.

The observables considered in this paper are correlators of Polyakov lines; it is well known that their signal to noise ratio is exponentially suppressed with the time-length of the lattice and with the spatial distance of the sources. For the pure gauge theory several techniques have been developed to overcome this problem for gluonic observables such as Polyakov loops, glueball interpolating operators, etc. [15–19]. In order to have a good statistical signal at large time distances, we opted for the multilevel algorithm proposed in Refs. [15–17].

The paper is organized as follows. In section II we collect the main aspects of the continuum theory: we summarize the results of Ref. [10], we discuss the rôle of the Gauss's law, we introduce the "color-twisted" and homogeneous boundary conditions and we collect the formulas relevant for the analysis of the numerical data. Section III is devoted to the lattice transcriptions of the previous formulas. The results of our simulations, in part reported in Ref. [20], are discussed in section IV, while in section V we draw our conclusions.

II. CONTINUUM THEORY

A. External sources

In order to compute the Feynman propagation kernel in a sector in which external q and $\bar{q}$ sources are present, we have to perform, in the continuum, the following operations [12]:

1. compute the propagation kernel with $A_0 = 0$

$$\tilde{K}(\mathbf{A}_2, \mathbf{A}_1; T) = \int_{\mathbf{A}(\mathbf{x},0)=\mathbf{A}_1(\mathbf{x})}^{\mathbf{A}(\mathbf{x},T)=\mathbf{A}_2(\mathbf{x})} \mathcal{D}\mathbf{A} \exp[-S_{YM}(\mathbf{A}, A_0 = 0)] \,, \tag{1}$$

as a functional of the initial $\mathbf{A}_1$ and final $\mathbf{A}_2$ gauge three-dimensional configurations. Eq. (1) describes a theory in which Gauss's law is not enforced.

2. enforce Gauss's law in presence of $q\bar{q}$ sources, through the integration over three-dimensional gauge transformations Ω

$$K(\mathbf{A}_2, s_2, r_2; \mathbf{A}_1, s_1, r_1; T) = \int_{\mathcal{G}_0} \mathcal{D}\Omega \, \Omega_{s_2 s_1}(\mathbf{x}_q) \, \Omega^*_{r_2 r_1}(\mathbf{x}_{\bar{q}}) \tilde{K}(\mathbf{A}_2^\Omega, \mathbf{A}_1; T) \,, \tag{2}$$

where

$$A_\mu^\Omega(x) \equiv \Omega^\dagger(x) \, A_\mu(x) \, \Omega(x) + i \, \Omega^\dagger(x) \, \partial_\mu \Omega(x) \,. \tag{3}$$

In Eq. (2) the $*$ denotes the complex conjugate, while s_1, s_2, r_1 and r_2 denote the initial and final color states of the q and the $\bar{q}$ sources, respectively. The domain $\mathcal{G}_0$ of the invariant measure integration is restricted to the topologically trivial gauge transformations which tend to 1 at three-dimensional infinity. In an infinite volume this is the condition needed in order not to eliminate from the Feynman propagation kernel the states with non-trivial global color content.

It is important to notice that when the theory is defined in a finite spatial volume with periodic boundary conditions, Gauss's law implies that the total color charge inside the volume carried by the gluons and the external sources is equal to the flux of the chromoelectric field through the boundary of the volume itself, and therefore vanishes identically as a consequence of periodicity. The color non-trivial states are therefore not present in the eigenspectrum of the finite volume theory with periodic boundary conditions, and a drastically different finite-size set up is needed to decide whether colored states can be excited or if their presence is suppressed as a consequence of the physics of color confinement.

The kernel K in Eq. (2) is related to the energy eigenvalues E_k and the corresponding energy eigenfunctionals $\psi_k(\mathbf{A}, s, r)$ by

$$K(\mathbf{A}_2, s_2, r_2; \mathbf{A}_1, s_1, r_1; T) = \sum_k e^{-E_k T} \psi_k(\mathbf{A}_2, s_2, r_2) \psi_k^*(\mathbf{A}_1, s_1, r_1) \,. \tag{4}$$

Under a gauge transformation $\Omega \in \mathcal{G}_0$, the states in Eq. (4) transform as

$$\psi_k(\mathbf{A}^\Omega, s, r) = (\Omega^\dagger(\mathbf{x}_q))_{ss'} \, (\Omega(\mathbf{x}_{\bar{q}}))_{r'r} \, \psi_k(\mathbf{A}, s', r') \,, \tag{5}$$

and the naive scalar product of two wave functionals is infinite. It must be replaced by the Faddeev-Popov gauge-fixed one

$$(\psi, \phi) = \int \mathcal{D}\mu_F(\mathbf{A}) \sum_{rs} \psi^*(\mathbf{A}, r, s) \, \phi(\mathbf{A}, r, s) \,, \tag{6}$$

where

$$\mathcal{D}\mu_F(\mathbf{A}) = \Delta_F(\mathbf{A}) \delta[F(\mathbf{A})] \delta\mathbf{A} \,, \tag{7}$$

and the Faddeev-Popov determinant $\Delta_F(\mathbf{A})$ is defined by [21]

$$\Delta_F(\mathbf{A}) \int_{\mathcal{G}_0} \mathcal{D}\Omega \, \delta[F(\mathbf{A}^\Omega)] = 1 \,. \tag{8}$$

As a consequence of Eq. (5), the value of the scalar product in Eq. (6) is independent from the choice of the gauge fixing functional $F(\mathbf{A})$. In the following we assume $F(\mathbf{A}) = \nabla \cdot \mathbf{A}$.

State	wave functional	orbital properties	ϕ at the null field conf.	global rep
singlet-singlet	$\psi^{(\mathbf{1},\mathbf{1})}(\mathbf{A};i,j)=\delta_{ij}\phi(\mathbf{A})$	$\phi(\mathbf{A}^V)=\phi(\mathbf{A})$	$\phi(\mathbf{0})\neq 0$	singlet
singlet-octet	$\psi^{(\mathbf{1},\mathbf{8})}(\mathbf{A};i,j)=\lambda^a_{ij}\phi^a(\mathbf{A})$	$\phi^a(\mathbf{A}^V)=\phi^a(\mathbf{A})$	$\phi^a(\mathbf{0})\neq 0$	octet
$\boldsymbol{\alpha}$-singlet	$\psi^{(\boldsymbol{\alpha},\mathbf{1})}_m(\mathbf{A};i,j)=\delta_{ij}\phi_m(\mathbf{A})$	$\phi_m(\mathbf{A}^V)=R^{\boldsymbol{\alpha}}_{mm'}(V)\phi_{m'}(\mathbf{A})$	$\phi_m(\mathbf{0})=0$	$\boldsymbol{\alpha}$
$\boldsymbol{\beta}$-octet	$\psi^{(\boldsymbol{\beta},\mathbf{8})}_m(\mathbf{A};i,j)=\lambda^a_{ij}\phi^a_m(\mathbf{A})$	$\phi^a_m(\mathbf{A}^V)=R^{\boldsymbol{\beta}}_{mm'}(V)\phi^a_{m'}(\mathbf{A})$	$\phi^a_m(\mathbf{0})=0$	$\boldsymbol{\gamma}\subset\boldsymbol{\beta}\otimes\mathbf{8}$

TABLE I: Classification of the color states with static $q\bar{q}$ sources. Every state is labeled by the orbital and the source representations respectively. The symbols $\boldsymbol{\alpha}$ and $\boldsymbol{\beta}$ indicate generic non-trivial representations.

B. Global color transformations and classification of states

A global color transformation V acts on the states as a unitary operator

$$[\mathcal{U}(V)\psi](\mathbf{A},s,r)=V_{ss'}V^*_{rr'}\psi(\mathbf{A}^V,s',r') \tag{9}$$

which commutes with the Hamiltonian [10]. If we re-organize the source indices in a matrix, the energy eigenstates in presence of $q\bar{q}$ sources can be written as

$$\psi(\mathbf{A},s,r)=[\phi(\mathbf{A})I+\lambda^a\phi^a(\mathbf{A})]_{sr}\equiv\psi_{sr}(\mathbf{A})\,, \tag{10}$$

where the traceless generators satisfy the normalization condition $\mathrm{Tr}[\lambda^a\lambda^b]=\delta^{ab}/2$, and the color rotations in Eq. (9) can be represented as

$$[\mathcal{U}(V)\psi](\mathbf{A})\equiv\psi^V(\mathbf{A})=V\psi(\mathbf{A}^V)V^\dagger=\phi(\mathbf{A}^V)I+V\lambda^aV^\dagger\phi^a(\mathbf{A}^V)\,. \tag{11}$$

Eq. (11) shows explicitly that the action of a color rotation results from a composition of a contribution coming from the action of V on the source indices and an "orbital" one coming from the transformation $\mathbf{A}\to\mathbf{A}^V$. In Tab. I we give the explicit classification of the color states. Several possible quantities can be computed, giving information about the structure of these states. In the following we classify them on the basis of the time boundary conditions.

C. Time-periodic boundary conditions

The simplest quantity to measure is the "total trace" over color source indices, i.e. the correlator of two Polyakov lines

$$\mathcal{K}(R,T)\equiv\int\mathcal{D}\mu_F(\mathbf{A})\sum_{s,r}K(\mathbf{A},s,r;\mathbf{A},s,r;T)=\sum_k d_k e^{-E_k(R)T}\,. \tag{12}$$

In Eq. (12) k runs over all the eigenstates of the Yang-Mills theory containing $q\bar{q}$ sources in all possible color configurations (see Table I); d_k is the multiplicity of the k-th level, and $E_k(R)$ is the corresponding energy which is a function of the relative spatial distance $R=|\mathbf{x}_q-\mathbf{x}_{\bar{q}}|$ between the two sources. The quantity $\sum_{s,r}K(\mathbf{A},s,r;\mathbf{A},s,r;T)$ is gauge invariant, and in the continuum the integration over $\mathbf{A}$ requires a gauge fixing. Following Ref. [10], we define the singlet and octet projectors on the color indices of the external sources

$$\Pi^{\mathbf{1}}_{s_2,r_2,s_1,r_1}=\frac{1}{3}\delta_{s_2r_2}\delta_{s_1r_1}, \tag{13}$$

$$\Pi^{\mathbf{8}}_{s_2,r_2,s_1,r_1}=2\sum_a\lambda^a_{r_2s_2}\lambda^a_{s_1r_1}=\delta_{s_2s_1}\delta_{r_2r_1}-\frac{1}{3}\delta_{s_2r_2}\delta_{s_1r_1}, \tag{14}$$

in terms of which we can define

$$\mathcal{K}_{\mathbf{1}}(R,T)=\int\mathcal{D}\mu_F(\mathbf{A})\sum_{s_2,r_2,s_1,r_1}\Pi^{\mathbf{1}}_{s_2,r_2,s_1,r_1}K(\mathbf{A},s_2,r_2;\mathbf{A},s_1,r_1;T)\,, \tag{15}$$

$$\mathcal{K}_{\mathbf{8}}(R,T)=\int\mathcal{D}\mu_F(\mathbf{A})\sum_{s_2,r_2,s_1,r_1}\Pi^{\mathbf{8}}_{s_2,r_2,s_1,r_1}K(\mathbf{A},s_2,r_2;\mathbf{A},s_1,r_1;T)\,. \tag{16}$$

The integrands in Eqs. (15) and (16) are not gauge invariant and require gauge fixing.

D. Color-twisted boundary conditions in time

In order to isolate the contributions from the various irreducible representations of the global color group, we introduce the color-twisted boundary conditions in the time direction requiring[1]

$$\mathbf{A}(\mathbf{x},T) = V^\dagger \mathbf{A}(\mathbf{x},0) V \,, \tag{17}$$

where V belongs to the global color group SU(3). An interesting quantity is [10]

$$\mathcal{K}(V,R,T) \equiv \sum_{s_1,s_2,r_1,r_2} \int \mathcal{D}\mu_F(\mathbf{A}) V_{s_1 s_2} V^*_{r_1 r_2} K(\mathbf{A}^V, s_2, r_2; \mathbf{A}, s_1, r_1; T) = \sum_{\boldsymbol{\alpha},k} \chi_{\boldsymbol{\alpha}}(V) e^{-E_k^{\boldsymbol{\alpha}}(R)T} \,, \tag{18}$$

where $\chi_{\boldsymbol{\alpha}}(V)$ denotes the character of V in the color representation $\boldsymbol{\alpha}$ to which the k-th level belongs. The contribution from the states transforming as an irreducible representation $\boldsymbol{\alpha}$ of the global color group are then given by

$$\mathcal{K}_{\boldsymbol{\alpha}}(R,T) = \dim_{\boldsymbol{\alpha}} \frac{\int DV\, \chi^*_{\boldsymbol{\alpha}}(V)\, \mathcal{K}(V,R,T)}{\int DV} \,, \tag{19}$$

where $\dim_{\boldsymbol{\alpha}}$ is the dimension of $\boldsymbol{\alpha}$. Another quantity of interest is the response of the propagation kernel to an "orbital" color rotation, defined as

$$\bar{\mathcal{K}}(V,R,T) \equiv \sum_{s,r} \int \mathcal{D}\mu_F(\mathbf{A})\, K(\mathbf{A}^V, s, r; \mathbf{A}, s, r; T) \,. \tag{20}$$

E. Homogeneous boundary conditions in time

In Refs. [10, 13] it is observed that in presence of the homogeneous boundary conditions

$$\mathbf{A}(\mathbf{x},T) = \mathbf{A}(\mathbf{x},0) = \mathbf{0} \tag{21}$$

only the singlet-singlet and singlet-octet states survive in the kernel because they are the only ones with a non-vanishing overlap with the null-field wave functional. Under these boundary conditions correlators of Polyakov lines are gauge invariant, and the octet projections of the kernel on the color external state representations can be computed without gauge fixing. We have, in this case,

$$\mathcal{K}^{(0)}(R,T) = \mathcal{K}^{(0)}_{\mathbf{1}}(R,T) + \mathcal{K}^{(0)}_{\mathbf{8}}(R,T) \,, \tag{22}$$

where

$$\mathcal{K}^{(0)}_{\mathbf{1}}(R,T) \equiv \frac{1}{3} \sum_{s,r} K(\mathbf{0},s,s;\mathbf{0},r,r;T) = \sum_k |\phi_k(\mathbf{0})|^2 e^{-E^{\mathbf{1}}_k(R)T} \,, \tag{23}$$

$$\mathcal{K}^{(0)}_{\mathbf{8}}(R,T) \equiv \sum_{s,r} K(\mathbf{0},s,r;\mathbf{0},s,r;T) - \frac{1}{3} \sum_{s,r} K(\mathbf{0},s,s;\mathbf{0},r,r;T) = 8 \sum_{a,k} |\phi^a_k(\mathbf{0})|^2 e^{-E^{\mathbf{8}}_k(R)T} \,, \tag{24}$$

and the superscript (0) denotes homogeneous boundary conditions.

III. LATTICE TRANSCRIPTION OF THE OBSERVABLES

On a lattice with periodic boundary conditions we are interested in the ratio of the various kernels, as defined in the previous section, normalized to the analogous one without external sources. In the case of Eq. (12) the ratio $W(R,T)$ is

$$W(R,T) = \left\langle \mathrm{Tr}(P(\mathbf{x}))\, \mathrm{Tr}(P^\dagger(\mathbf{y})) \right\rangle_T \,, \qquad R = |\mathbf{x}_q - \mathbf{x}_{\bar{q}}| \tag{25}$$

---

[1] In Ref. [19] analogous boundary conditions were considered for the construction of the projectors onto irreducible representations of the global symmetry groups of the Yang–Mills theory.

where the Polyakov line $P(\mathbf{x})$ is defined by

$$P(\mathbf{x}) = \prod_{x_0=0}^{T-1} U_0(\mathbf{x}, x_0)\,, \tag{26}$$

and $U_\mu(x)$ is the link matrix located at the position x pointing toward the positive μ direction. Under a gauge transformation the trace over the color index $\mathrm{Tr}(P(\mathbf{x}))$ is invariant, and, on the lattice, gauge fixing is not required to compute $W(R,T)$. The correlators corresponding to the quantities in Eqs. (15) and (16) are

$$W_{\mathbf{1}}(R,T) = \frac{1}{3}\left\langle \mathrm{Tr}(P(\mathbf{x})P^\dagger(\mathbf{y}))\right\rangle_T \tag{27}$$

$$W_{\mathbf{8}}(R,T) = \left\langle \mathrm{Tr}(P(\mathbf{x}))\mathrm{Tr}(P^\dagger(\mathbf{y}))\right\rangle_T - \frac{1}{3}\left\langle \mathrm{Tr}(P(\mathbf{x})P^\dagger(\mathbf{y}))\right\rangle_T\,, \tag{28}$$

where it is understood that Coulomb's gauge on the time slice at $x_0 = 0$ must be fixed, see for instance Ref. [22].

Twisted boundary conditions in the temporal direction are introduced by requiring that

$$U_\mu(\mathbf{x}, T) = V^\dagger U_\mu(\mathbf{x}, 0) V\,. \tag{29}$$

The correlators associated to the quantities $\mathcal{K}(V,R,T)$ and $\bar{\mathcal{K}}(V,R,T)$ in Eqs. (18) and (20) are defined as

$$W(V,R,T) = \left\langle \mathrm{Tr}(VP(\mathbf{x}))\,\mathrm{Tr}(V^\dagger P^\dagger(\mathbf{y}))\right\rangle_{T,V}\,, \qquad \overline{W}(V,R,T) = \left\langle \mathrm{Tr}(P(\mathbf{x}))\,\mathrm{Tr}(P^\dagger(\mathbf{y}))\right\rangle_{T,V}\,, \tag{30}$$

where the subscript V indicates that the path integral integration is performed in presence of color-twisted boundary conditions, Eq. (29).

Finally, homogeneous boundary conditions are defined by

$$U_0(\mathbf{x}, T) = U_0(\mathbf{x}, 0) = \mathbb{1}\,, \tag{31}$$

and the definitions of the lattice correlators $W^{(0)}(R,T)$, $W^{(0)}_{\mathbf{1}}(R,T)$, $W^{(0)}_{\mathbf{8}}(R,T)$ follow straightforwardly from Eqs. (22), (23) and (24).

IV. NUMERICAL RESULTS

The SU(3) Yang-Mills theory is discretized with the Wilson action. Numerical computations are performed by standard Monte Carlo techniques alternating 1 heat-bath with 5 over-relaxation steps. In the following the effective energy extracted from a correlator is defined as

$$\mathcal{E}(R,T) = \frac{1}{\Delta}\ln\left[\frac{W(R,T-\Delta)}{W(R,T)}\right]\,, \tag{32}$$

where $\Delta = 4$ unless $T = 8$ for which $\Delta = 2$.

A. Color-twisted boundary conditions

We computed the dependence of $W(V,R,T)$ and $\bar{W}(V,R,T)$ defined in Eq. (30), at fixed T and for different values of R, as a function of the octet character $\chi_{\mathbf{8}}(V) = |\mathrm{Tr}(V)|^2 - 1$. This run was carried out on a rather small volume, $10^3 \times 4$ at $\beta = 6.0$, in order to be able to keep under control the statistical noise without the necessity of using the multilevel technique. The number of generated configurations and the corresponding values of $\chi_{\mathbf{8}}(V)$ are listed in Tab. II. The values of $W(V,R,T)$ are independent from the character $\chi_{\mathbf{8}}(V)$ at fixed values of R, see Fig. 1a. This is consistent with the expectation that in presence of periodic boundary conditions every state contributing to the propagation kernel is a global color singlet. The states in the octet external source sector, which contribute to the projected Feynman kernel in Eq. (28), are therefore in an orbital-octet representation so to form an overall global singlet. This fact is numerically confirmed by the computation of $\overline{W}(V,R,T)$, as shown in Fig. 1b which exhibits the linear dependence on the adjoint character of V typical of states in an orbital octet representation.

$\chi_{\mathbf{8}}(V)$	# of confs.	$\chi_{\mathbf{8}}(V)$	# of confs.
−0.96	10000	5.25	4293
−0.46	16000	6.41	2453
0.37	4000	6.77	4000
1.12	16000	7.0	4000
2.8	16000	8.0	2000

TABLE II: Number of configurations generated and the corresponding value of the adjoint character $\chi_{\mathbf{8}}(V)$ of the SU(3) matrix at the boundary. Notice that $-1 < \chi_{\mathbf{8}}(V) \leq 8$.

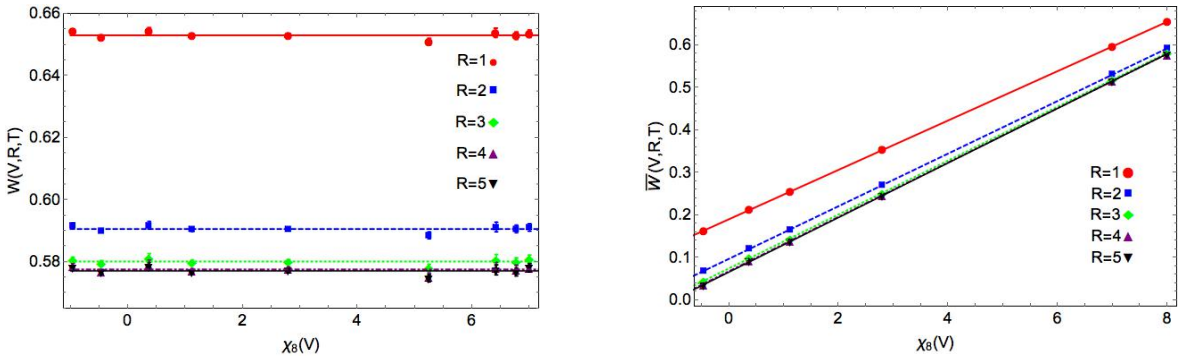

(a) (b)

FIG. 1: $W(V,R,T)$ (a) and $\overline{W}(V,R,T)$ (b) as a function of the adjoint character $\chi_{\mathbf{8}}(V)$.

B. Periodic boundary conditions

In order to compute the lowest energy eigenvalues of the states contributing to the correlators, the time extension T of the lattice has been chosen large enough for the excited states to give a negligible contribution with respect to the statistical errors. For this purpose, 200 independent configurations with $\beta = 5.7$, volume $12^3 \times T$, for $T = 6, 8, 12, 16, 20$ have been generated. Each of these configurations has been taken as the starting point for the multi-level averaging. The numerical values for the singlet and octet correlators $W_{\mathbf{1}}(R,T)$ and $W_{\mathbf{8}}(R,T)$ are reported in Tab V and Tab. VI of the Appendix A, respectively. We computed the effective energies $\mathcal{E}_{\mathbf{1}}(R,T)$ and $\mathcal{E}_{\mathbf{8}}(R,T)$ for the singlet and the octet correlator as a function of T at a given separation R. The results are shown in Figs. 2a and 2b, while their values at $T = 20$ are reported in Table III. We assume the value of the effective energies computed at $T = 20$ as our best numerical estimates.

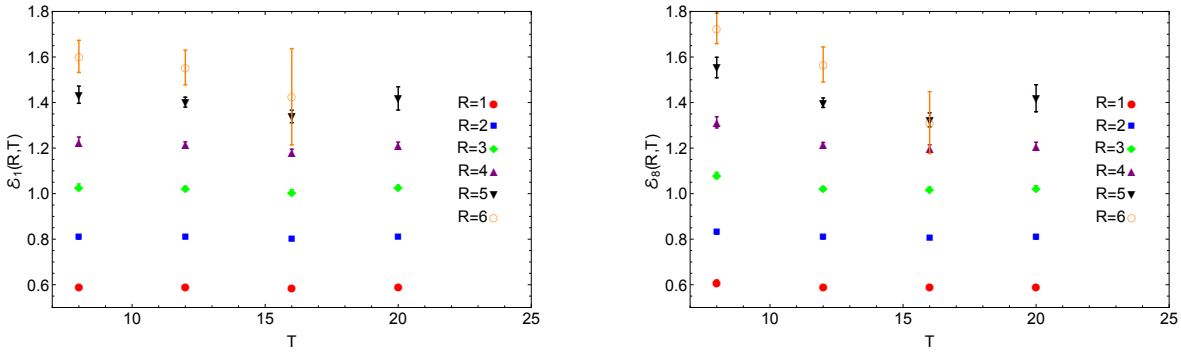

(a) (b)

FIG. 2: Effective energies $\mathcal{E}_{\mathbf{1}}(R,T)$ (a) and $\mathcal{E}_{\mathbf{8}}(R,T)$ (b) as a function of the temporal extension T of the lattice for $R = 1 \div 6$. The quantity Δ is equal to 4 except for $T = 8$ for which is 2.

R	$\mathcal{E}_{\mathbf{1}}(R,20)$	$\mathcal{E}_{\mathbf{8}}(R,20)$
1	$(5.93 \pm 0.02) \times 10^{-1}$	$(5.91 \pm 0.05) \times 10^{-1}$
2	$(8.10 \pm 0.05) \times 10^{-1}$	$(8.07 \pm 0.06) \times 10^{-1}$
3	1.029 ± 0.009	1.025 ± 0.010
4	1.21 ± 0.01	1.21 ± 0.01
5	1.42 ± 0.05	1.42 ± 0.06

TABLE III: The values of $\mathcal{E}_{\mathbf{1}}(R,20)$ and $\mathcal{E}_{\mathbf{8}}(R,20)$ as a function of the distance.

We find that the singlet-singlet and octet-octet energies coincide within statistical errors. This confirms that the ground state is a unique global color singlet with non-trivial components on the $q\bar{q}$ octet and singlet external source sectors.

C. Homogeneous boundary conditions

As remarked above, the use of homogeneous boundary conditions in the time direction allows the computation of singlet and octet source index correlators without the need of gauge-fixing. As in section IV B, we generated

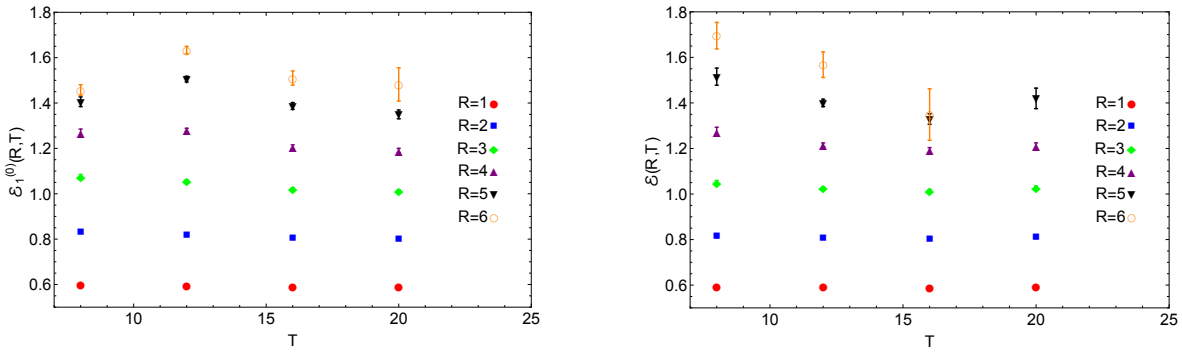

(a) (b)

FIG. 3: Effective energies $\mathcal{E}_{\mathbf{1}}^{(0)}(R,20)$ (a) and $\mathcal{E}(R,20)$ (b) as a function of the temporal extension T of the lattice for $R = 1 \div 6$. The quantity Δ is equal to 4 except for $T = 8$ for which is 2.

200 configurations on which we applied the multilevel. As compared with $W(R,T)$, $W_{\mathbf{1}}^{(0)}(R,T)$ turns out to have a larger pre-factor as can be seen comparing the values of the kernel in Tab. VIII with those in Tab. V. In Figs. 3a and 3b we show the results for the effective energy $\mathcal{E}_{\mathbf{1}}^{(0)}(R,T)$ of $W_{\mathbf{1}}^{(0)}(R,T)$ and for the effective energy $\mathcal{E}(R,T)$ of the gauge invariant $W(R,T)$ with periodic boundary conditions. The effective energies at $T = 20$ are also reported in Table IV.

We find that the values extracted in the two cases are compatible within statistical errors, and that they are consistent with those computed in the previous sub-section, see Table III. The correlator $K_{\mathbf{8}}^{(0)}(R,T)$ is compatible with zero within statistical errors. This confirms the fact that only the singlet external source projection has a non-vanishing overlap with the null-field wave functional.

V. CONCLUSIONS

In this paper we have discussed the color structure of the Yang-Mills states in the presence of $q\bar{q}$ static quark sources with periodic boundary conditions in the spatial directions and periodic, color-twisted and homogeneous boundary conditions in the temporal one. A multilevel simulation algorithm has been necessary to obtain precise results on lattices corresponding to large times. From the outcome of our computations a general picture emerges for the structure of states in sectors with external sources. The states contributing to the Feynman propagation

R	$\mathcal{E}_{\mathbf{1}}^{(0)}(R,20)$	$\mathcal{E}(R,20)$
1	$(5.90 \pm 0.02) \times 10^{-1}$	$(5.93 \pm 0.02) \times 10^{-1}$
2	$(8.01 \pm 0.04) \times 10^{-1}$	$(8.09 \pm 0.05) \times 10^{-1}$
3	1.011 ± 0.007	1.028 ± 0.008
4	1.19 ± 0.01	1.21 ± 0.01
5	1.34 ± 0.02	1.42 ± 0.04

TABLE IV: The values of $\mathcal{E}_{\mathbf{1}}^{(0)}(R,20)$ and $\mathcal{E}(R,20)$ as a function of the distance.

kernel are global color singlets only. Our interpretation is that this fact does not necessarily have a dynamical meaning related to confinement, but is rather due to the periodic quantization conditions imposed in the spatial volume. We conclude that the states are of the form referred to as singlet-singlet or octet-octet. Of course, any mixing between these two cases is allowed, and only dynamical considerations can determine their relative weight in a quantitative way. Our numerical results are consistent with the observation that only the singlet external source contribution has a non-vanishing overlap with the null-field wave functional.

In view of the recent developments of the phenomenology of tetraquark (see for a review Ref. [23]) and pentaquark [24] states we are undertaking the study of the non perturbative effective potentials acting in these channels, using the techniques described in the present paper.

ACKNOWLEDGMENTS

We thank Giancarlo Rossi for many discussions and suggestions.

Appendix A: Numerical results for the correlators

In this appendix we report the values of the correlators as a function of the distance between the external sources R and the temporal extension T computed with the multilevel algorithm. The errors are estimated using the jackknife method.

R	$W_{\mathbf{1}}(R,6)$	$W_{\mathbf{1}}(R,8)$	$W_{\mathbf{1}}(R,12)$	$W_{\mathbf{1}}(R,16)$	$W_{\mathbf{1}}(R,20)$
1	$(2.666 \pm 0.007) \times 10^{-2}$	$(8.19 \pm 0.03) \times 10^{-3}$	$(7.72 \pm 0.03) \times 10^{-4}$	$(7.25 \pm 0.03) \times 10^{-5}$	$(6.82 \pm 0.03) \times 10^{-6}$
2	$(6.28 \pm 0.04) \times 10^{-3}$	$(1.254 \pm 0.009) \times 10^{-3}$	$(5.05 \pm 0.04) \times 10^{-5}$	$(2.02 \pm 0.02) \times 10^{-6}$	$(8.04 \pm 0.09) \times 10^{-8}$
3	$(1.42 \pm 0.02) \times 10^{-3}$	$(1.82 \pm 0.02) \times 10^{-4}$	$(3.11 \pm 0.04) \times 10^{-6}$	$(5.28 \pm 0.09) \times 10^{-8}$	$(8.86 \pm 0.18) \times 10^{-10}$
4	$(3.78 \pm 0.06) \times 10^{-4}$	$(3.29 \pm 0.06) \times 10^{-5}$	$(2.68 \pm 0.06) \times 10^{-7}$	$(2.19 \pm 0.06) \times 10^{-9}$	$(1.79 \pm 0.06) \times 10^{-11}$
5	$(1.15 \pm 0.04) \times 10^{-4}$	$(6.6 \pm 0.2) \times 10^{-6}$	$(2.7 \pm 0.1) \times 10^{-8}$	$(1.03 \pm 0.07) \times 10^{-10}$	$(4.2 \pm 0.5) \times 10^{-13}$
6	$(6.3 \pm 0.4) \times 10^{-5}$	$(2.5 \pm 0.2) \times 10^{-6}$	$(6.0 \pm 0.9) \times 10^{-9}$	$(3.7 \pm 6.9) \times 10^{-12}$	$(5.1 \pm 4.9) \times 10^{-14}$

TABLE V: Singlet projected correlator computed with the gauge-fixing and periodic boundary conditions.

R	$W_{\mathbf{8}}(R,6)$	$W_{\mathbf{8}}(R,8)$	$W_{\mathbf{8}}(R,12)$	$W_{\mathbf{8}}(R,16)$	$W_{\mathbf{8}}(R,20)$
1	$(2.42 \pm 0.02) \times 10^{-3}$	$(7.11 \pm 0.06) \times 10^{-4}$	$(6.63 \pm 0.06) \times 10^{-5}$	$(6.22 \pm 0.06) \times 10^{-6}$	$(5.88 \pm 0.06) \times 10^{-7}$
2	$(1.92 \pm 0.02) \times 10^{-3}$	$(3.64 \pm 0.03) \times 10^{-4}$	$(1.44 \pm 0.01) \times 10^{-5}$	$(5.74 \pm 0.07) \times 10^{-7}$	$(2.31 \pm 0.03) \times 10^{-8}$
3	$(9.4 \pm 0.1) \times 10^{-4}$	$(1.09 \pm 0.01) \times 10^{-4}$	$(1.82 \pm 0.02) \times 10^{-6}$	$(3.04 \pm 0.05) \times 10^{-8}$	$(5.18 \pm 0.10) \times 10^{-10}$
4	$(4.8 \pm 0.1) \times 10^{-4}$	$(3.56 \pm 0.07) \times 10^{-5}$	$(2.76 \pm 0.05) \times 10^{-7}$	$(2.21 \pm 0.06) \times 10^{-9}$	$(1.81 \pm 0.05) \times 10^{-11}$
5	$(2.7 \pm 0.2) \times 10^{-4}$	$(1.27 \pm 0.04) \times 10^{-6}$	$(4.6 \pm 0.2) \times 10^{-8}$	$(1.9 \pm 0.2) \times 10^{-10}$	$(7.2 \pm 0.1) \times 10^{-13}$
6	$(2.1 \pm 0.1) \times 10^{-4}$	$(7.3 \pm 0.4) \times 10^{-6}$	$(1.4 \pm 0.3) \times 10^{-8}$	$(2.2 \pm 1.9) \times 10^{-11}$	–

TABLE VI: Octet projected correlator computed with the gauge-fixing and periodic boundary conditions.

R	$W(R,6)$	$W(R,8)$	$W(R,12)$	$W(R,16)$	$W(R,20)$
1	$(2.908 \pm 0.006) \times 10^{-2}$	$(8.90 \pm 0.02) \times 10^{-3}$	$(8.39 \pm 0.03) \times 10^{-4}$	$(7.87 \pm 0.03) \times 10^{-5}$	$(7.41 \pm 0.04) \times 10^{-6}$
2	$(8.20 \pm 0.04) \times 10^{-3}$	$(1.62 \pm 0.01) \times 10^{-3}$	$(6.50 \pm 0.04) \times 10^{-5}$	$(2.59 \pm 0.02) \times 10^{-6}$	$(1.04 \pm 0.01) \times 10^{-7}$
3	$(2.36 \pm 0.02) \times 10^{-3}$	$(2.92 \pm 0.03) \times 10^{-4}$	$(4.94 \pm 0.06) \times 10^{-6}$	$(8.32 \pm 0.13) \times 10^{-8}$	$(1.40 \pm 0.03) \times 10^{-9}$
4	$(8.6 \pm 0.2) \times 10^{-4}$	$(6.90 \pm 0.11) \times 10^{-5}$	$(5.43 \pm 0.09) \times 10^{-7}$	$(4.4 \pm 0.1) \times 10^{-9}$	$(3.59 \pm 0.10) \times 10^{-11}$
5	$(3.9 \pm 0.1) \times 10^{-4}$	$(1.93 \pm 0.06) \times 10^{-5}$	$(7.3 \pm 0.3) \times 10^{-8}$	$(3.0 \pm 0.2) \times 10^{-10}$	$(1.1 \pm 0.1) \times 10^{-12}$
6	$(2.8 \pm 0.1) \times 10^{-4}$	$(9.8 \pm 0.5) \times 10^{-6}$	$(2.1 \pm 0.3) \times 10^{-8}$	$(2.6 \pm 2.0) \times 10^{-11}$	–

TABLE VII: Total trace correlator in presence of periodic boundary conditions.

R	$W_{\mathbf{1}}^{(0)}(R,6)$	$W_{\mathbf{1}}^{(0)}(R,8)$	$W_{\mathbf{1}}^{(0)}(R,12)$	$W_{\mathbf{1}}^{(0)}(R,16)$	$W_{\mathbf{1}}^{(0)}(R,20)$
1	$(5.065 \pm 0.003) \times 10^{-2}$	$(1.154 \pm 0.003) \times 10^{-2}$	$(1.424 \pm 0.004) \times 10^{-3}$	$(1.346 \pm 0.005) \times 10^{-4}$	$(1.265 \pm 0.005) \times 10^{-5}$
2	$(2.713 \pm 0.003) \times 10^{-2}$	$(5.17 \pm 0.03) \times 10^{-3}$	$(1.96 \pm 0.01) \times 10^{-4}$	$(7.86 \pm 0.06) \times 10^{-6}$	$(3.15 \pm 0.03) \times 10^{-7}$
3	$(1.684 \pm 0.003) \times 10^{-2}$	$(1.97 \pm 0.02) \times 10^{-3}$	$(2.91 \pm 0.03) \times 10^{-5}$	$(4.89 \pm 0.07) \times 10^{-7}$	$(8.38 \pm 0.13) \times 10^{-9}$
4	$(1.322 \pm 0.003) \times 10^{-2}$	$(1.04 \pm 0.02) \times 10^{-3}$	$(6.33 \pm 0.11) \times 10^{-6}$	$(5.01 \pm 0.10) \times 10^{-8}$	$(4.19 \pm 0.10) \times 10^{-10}$
5	$(1.172 \pm 0.003) \times 10^{-2}$	$(6.87 \pm 0.16) \times 10^{-4}$	$(1.70 \pm 0.04) \times 10^{-6}$	$(6.4 \pm 0.2) \times 10^{-9}$	$(2.8 \pm 0.1) \times 10^{-11}$
6	$(1.130 \pm 0.003) \times 10^{-2}$	$(5.93 \pm 0.16) \times 10^{-4}$	$(8.5 \pm 0.3) \times 10^{-7}$	$(1.7 \pm 0.1) \times 10^{-9}$	$(5.1 \pm 0.8) \times 10^{-12}$

TABLE VIII: Singlet projected correlator computed in presence of homogeneous boundary conditions.

[1] L. S. Brown and W. I. Weisberger, Phys. Rev. D **20**, 3239 (1979).
[2] L. D. McLerran and B. Svetitsky, Phys. Rev. D **24**, 450 (1981).
[3] S. Nadkarni, Phys. Rev. D **34**, 3904 (1986).
[4] G. T. Bodwin, E. Braaten and G. P. Lepage, Phys. Rev. D **51**, 1125 (1995) [Erratum-ibid. D **55**, 5853 (1997)] [hep-ph/9407339].
[5] E. V. Shuryak and I. Zahed, Phys. Rev. D **70**, 054507 (2004) [hep-ph/0403127].
[6] G. S. Bali and A Pineda, Phys. Rev. D **69**, 094001 (2004).
[7] O. Philipsen, Phys. Lett. B **535**, 138 (2002) [hep-lat/0203018],
[8] O. Jahn and O. Philipsen, Phys. Rev. D **70**, 074504 (2004) [hep-lat/0407042],
[9] O. Philipsen and M. Wagner, Phys. Rev. D **89**, 014509 (2014).
[10] G. C. Rossi and M. Testa, Phys. Rev. D **87**, no. 8, 085014 (2013) [arXiv:1304.2542 [hep-lat]].
[11] G. C. Rossi and M. Testa, PoS LATTICE **2013**, 369 (2014) [arXiv:1309.4941 [hep-lat]].
[12] G. C. Rossi and M. Testa, Nucl. Phys. B **163**, 109 (1980).
[13] G. C. Rossi and M. Testa, Nucl. Phys. B **176**, 477 (1980).
[14] G. C. Rossi and M. Testa, Nucl. Phys. B **237**, 442 (1984).
[15] G. Parisi, R. Petronzio and F. Rapuano, Phys. Lett. B **128**, 418 (1983).
[16] M. Luscher and P. Weisz, JHEP **0109**, 010 (2001) [hep-lat/0108014].
[17] M. Luscher and P. Weisz, JHEP **0207**, 049 (2002) [hep-lat/0207003].
[18] H. B. Meyer, JHEP **0401** (2004) 030 [hep-lat/0312034].
[19] M. Della Morte and L. Giusti, JHEP **1105** (2011) 056 [arXiv:1012.2562 [hep-lat]].
[20] A. L. Guerrieri, S. Petrarca, A. Rubeo and M. Testa, PoS LATTICE **2013**, 470 (2014) [arXiv:1311.1325 [hep-lat]].
[21] L. D. Faddeev and V. N. Popov, Phys. Lett. B **25**, 29 (1967).
[22] L. Giusti, M. L. Paciello, C. Parrinello, S. Petrarca and B. Taglienti, Int. J. Mod. Phys. A **16** (2001) 3487 [hep-lat/0104012].
[23] A. Esposito, A. L. Guerrieri, F. Piccinini, A. Pilloni and A. D. Polosa, Int. J. Mod. Phys. A **30**, 1530002 (2014) [arXiv:1411.5997 [hep-ph]].
[24] LHCb collaboration, CERN-PH-EP-2015-153, LHCb-PAPER-2015-029 [arXiv:1507.03414v2 [hep-ex]].